Photochemical & Photobiological Sciences

Accepted Manuscript

This is an *Accepted Manuscript*, which has been through the Royal Society of Chemistry peer review process and has been accepted for publication.

Accepted Manuscripts are published online shortly after acceptance, before technical editing, formatting and proof reading. Using this free service, authors can make their results available to the community, in citable form, before we publish the edited article. We will replace this *Accepted Manuscript* with the edited and formatted *Advance Article* as soon as it is available.

You can find more information about *Accepted Manuscripts* in the Information for Authors.

Please note that technical editing may introduce minor changes to the text and/or graphics, which may alter content. The journal's standard Terms & Conditions and the Ethical guidelines still apply. In no event shall the Royal Society of Chemistry be held responsible for any errors or omissions in this *Accepted Manuscript* or any consequences arising from the use of any information it contains.

ROYAL SOCIETY OF CHEMISTRY

www.rsc.org/pps

Journal Name

RSCPublishing

ARTICLE

Anion Exchange Nanofiber Materials Activated by Daylight with a Dual Antibacterial Effect†

Cite this: DOI: 10.1039/xoxxoooooox

L. Plíštil,[ab] P. Henke,[a] P. Kubát,[c] and J. Mosinger*[ad]

Received ooth January 2012,
Accepted ooth January 2012

DOI: 10.1039/xoxxoooooox

www.rsc.org/

Anion exchange polystyrene nanofiber materials (**AE**) were prepared by electrospinning followed by two-step functionalization of the nanofiber surface by chlorosulfonic acid and ethylendiamine. The photoactive character of these materials was introduced through adsorption of the tetra-anionic 5,10,15,20-tetrakis-(4-sulfonatophenyl)porphyrin photosensitizer (**TPPS-AE**) on the nanofiber surface or by encapsulation of the nonpolar 5,10,15,20-tetraphenylporphyrin photosensitizer (**AE(TPP)**) into the nanofibers. Anion exchange nanofiber materials with porphyrins are characterized by a high ion-exchange capacity, photogeneration of singlet oxygen $O_2(^1\Delta_g)$, and singlet oxygen-sensitized delayed fluorescence. Due to the photogeneration of cytotoxic $O_2(^1\Delta_g)$, the nanofibers exhibited oxidation of the external substrates in aqueous solutions and an efficient antibacterial effect when activated by simulated daylight. Adsorption of both TPPS and I^- on the surface of **AE** led to the formation of more efficient **I-TPPS-AE** materials. Rapid photooxidation of I^- by $O_2(^1\Delta_g)$, and the formation of another cytotoxic species, I_3^-, on the surface of the nanofibers were responsible for the increased antibacterial properties of **I-TPPS-AE** and the prolonged antibacterial effect in the dark.

Introduction

During the past two decades, there has been an increasing number of studies on polymer nanofibers and their applications as filtration materials,[1] carriers for catalytic reactions,[2] optical sensors,[3] smart textiles,[4] nanofiber-based scaffolds for the regeneration of bone, skin, heart, and blood vessels[5-7], and multifunctional devices[8] due to their excellent properties, including a high surface/weight ratio, high flexibility, and low cost. Although many techniques have been developed to fabricate polymer nanofibers,[7] the most common method is electrospinning from a polymer solution.[9]

Previously, we reported on photoactive electrospun polymer nanofiber materials with encapsulated nonpolar photosensitizers that generate $O_2(^1\Delta_g)$ upon irradiation with visible light. Short-living, highly cytotoxic $O_2(^1\Delta_g)$ photogenerated primarily inside the nanofibers efficiently kills bacteria, including *Escherichia coli, Staphylococcus aureus,* and *Pseudomonas aeruginosa*[10-13], as well as non-enveloped polyomaviruses and enveloped baculoviruses[14] on the surface of such nanofiber materials without any leaching of the photosensitizer. The photoactive nanofiber materials were characterized by a high surface area, transparency to light, a high oxygen permeability/diffusion, and a nanoporous structure,[9,15] which disables bacteria to pass through the materials as they are detained on the surface.[16]

The small diameter of nanofibers allows for the diffusion of $O_2(^1\Delta_g)$ outside of the nanofibers from a polymer with higher oxygen permeability/diffusion and for photooxidation of a chemical substrate or biological targets.[17,18] The main issue associated with polymeric nanofiber materials with encapsulated photosensitizers is the low diffusing length of $O_2(^1\Delta_g)$ (typically tens to hundreds of nm),[19] which limits efficient photooxidation and antimicrobial action in close proximity to nanofiber surfaces. To overcome this issue, we prepared sulfonated polystyrene nanofibers with externally, ionically bounded tetra-cationic photosensitizers.[16]

Because most of the commonly used water-soluble photosensitizers have an anionic character, we prepared anion exchange electrospun polystyrene nanofiber materials with modified surfaces. The efficient photooxidation and antibacterial character of nanofibers were introduced into these materials through adsorption of the tetra-anionic 5,10,15,20-tetrakis-(4-sulfonatophenyl) porphyrin (TPPS) photosensitizer. The properties of **TPPS-AE** were compared with the anion exchange nanofibers with an encapsulated nonpolar 5,10,15,20-tetraphenylporphyrin (TPP) photosensitizer **AE(TPP)** and **PS(TPP)** (TPP encapsulated in polystyrene (**PS**) nanofibers) starting material used in previous studies.[12]

Experimental Section

Chemicals

5,10,15,20-Tetraphenylporphyrin (TPP), 5,10,15,20-tetrakis-(4-sulfonatophenyl)porphyrin (TPPS), (tetraethylammonium bromide (TEAB), chlorosulfonic acid, ethylenediamine (EDA), LB agar, LB medium, and KI were purchased from Sigma-Aldrich and used as received. Cyclohexanone and dichloromethane were purchased from Penta (Czech Republic) and used as received. Polystyrene Synthos PS GP 137 was purchased from Synthos Kralupy (Czech Republic).

Electrospinning

The nanofiber materials were prepared using the modified Nanospider™ electrospinning technology. This method enables the simultaneous formation of charged liquid jets on the surface of a thin wire electrode, and the number and location of the jets are set up naturally in their optimal positions.[20] The polystyrene solution for electrospinning was prepared as follows: 82 g of cyclohexanone, 17.9 g of polystyrene, and 0.072 g of TEAB (for the **PS** nanofiber material) or the same composition plus 0.18 g of TPP (for the **PS(TPP)** nanofiber material) were magnetically stirred and heated (60°C) to complete dissolution (approximately 4 h). The obtained polymer solution was then cooled to room temperature and electrospun at 80 kV, with a 200 mm distance between electrodes at 30% relative humidity and 22°C. Polypropylene antistatic spunbond (20-30 g/m^2, Atex, Italy) was used as the carrier material for the nanofiber collection, moving at a speed of 200 mm/min.

Preparation of the anion-exchange nanofiber material

The pieces (5.2×5 cm) of electrospun PS nanofiber material (approximately 6 mg) were fixed on a glass substrate and dipped in chlorosulfonic acid at ambient temperature for 1-20 min. The layers were subsequently washed with dichloromethane and reacted with ethylenediamine (EDA) for 1-20 min. The obtained anion-exchange polystyrene nanofiber material (**AE**) was transformed to the chloride form in 0.1% (27 mM) HCl, rinsed with deionized water to neutrality, and stored in deionized water.

Ion exchange capacity (IEC)

The IEC of the **AE** material was determined by acidobasic titration. Approximately 40 mg of the AE material in chloride form was treated with 20 mL of 10 mM NaOH solution for 1 day. The remaining NaOH was titrated potentiometrically with 10 mM HCl. The IECs were related to the mass of the dried materials.

Adsorption of TPPS and I$^-$

Next, 10 mg (5.2×5 cm^2) of **AE** with an IEC of 2.5 mmol/g was immersed in demi water for one day and then in 25 mL of the aqueous solution of TPPS and gently shaken (30 rpm) for 24 h to ensure complete saturation of the anion-exchange sites (monitored by UV-Vis spectroscopy). The concentrations of the TPPS solutions were 10^{-6}, 10^{-5}, and 10^{-4} M. The final molar ratios of TPPS vs. the ion exchange sites (IESs) in the resulting **TPPS-AE** were 0.001, 0.01, and 0.1, respectively. For the preparation of samples with adsorbed iodide (**I-TPPS-AE**), 10 mg of **TPPS-AE** with medium loading (TPPS/IES = 0.01) was immersed in a 1 mM solution of KI and shaken overnight at 30 rpm. The samples were washed with deionized water until the iodide absorption peak at 227 nm was no longer observed using UV-Vis spectroscopy.

Preparation of the triiodide solution

In this step, 0.0165 g (0.1 mmol) of KI and 0.0254 g (0.1 mmol) of I_2 were magnetically stirred overnight in 100 mL of deionized water to complete dissolution. The resulting concentration of I_3^- ions was determined by UV-Vis absorption spectroscopy (ε_{287} = 40000 M^{-1}cm^{-1}, ε_{351} = 26000 M^{-1}cm^{-1}) and observed to be 0.065 mM.

Measurement of adsorption kinetics

Three aqueous solutions were used for the adsorption kinetic measurements with the same concentration of charges: 1.6 μM of TPPS, 6.4 μM of I_3^-, and 6.4 μM of KI. Next, 20 mL of the desired solution was poured into a beaker with a 6 cm^2 piece of **AE** nanofiber material (IEC = 4.0 mmol g^{-1}) on a quartz plate. The solution was then pumped through a cyclic continuous flow cuvette system at a constant flow rate of 20 mL/min. The adsorption was monitored by UV-Vis absorption spectroscopy at 414 nm (TPPS), 351 nm (I_3^-), and 227 nm (I^-).

Scanning electron microscopy (SEM)

The morphologies of the nanofiber materials were analyzed with a scanning electron microscope (FEI Quanta 200, USA) at high vacuum using an Everhart-Thornley secondary electron detector and gold as a conductive agent. The mean diameter of the obtained nanofibers was estimated using NIS Elements 4.0 image analysis software (Laboratory Imaging, Czech Republic). Five samples were acquired from the nanofiber material, and at least 50 individual nanofiber diameters were measured from each sample.

Apparent contact angle measurements

The hydrophobic/hydrophilic character of the PS surfaces was characterized by apparent contact angle (ACA) measurements using a Surface Energy Evaluation System (See System Standard, Czech Republic). The ACAs of the surfaces were measured using a 3 μL deionized water droplet. Each measurement was repeated five times to obtain the average value of the contact angle calculated by multipoint fitting of the drop profile using the SEES software.

Steady-state absorption and fluorescence spectroscopy

The UV-Vis absorption spectra were recorded on a Cary 4000 spectrometer equipped with an integration sphere. The sample of nanofiber material (one layer on a quartz plate) was placed at the entrance to the sphere and measured in the diffuse transmittance mode to minimize light scattering. The UV-Vis

fluorescence spectra were monitored on an Aminco Bowman (AB2) spectrophotometer. All of the fluorescence emission spectra were corrected for the characteristics of the detection monochromator and photomultiplier using fluorescence standards.

Fourier transform infrared (FTIR) spectra.

FTIR spectra were collected in the transmission mode using a Thermo Scientific FTIR spectrometer (Nicolet 6700) with Happ-Genzel apodization in the 400-4000 cm^{-1} range.

Porphyrin triplet states, singlet oxygen, and singlet oxygen-sensitized delayed fluorescence (SODF).

The samples were excited by a FL 3002 dye laser (422 nm, output energy 0.1-3 mJ/pulse, pulse width ~28 ns) and by a COMPEX102 XeCl excimer laser (308 nm, both Lambda Physik). The time profiles of the porphyrin triplet states (average of 5-250 traces) were probed by transient absorption at 480 nm using a 150 W Xe lamp (Phillips) equipped with a pulse unit and an R928 photomultiplier (Hamamatsu). The lifetimes of the porphyrin triplet states (τ_T) were determined using a single exponential fit.

The formation of singlet oxygen, $O_2(^1\Delta_g)$, was observed by time-resolved near-infrared phosphorescence at 1270 nm. The phosphorescence was monitored with a germanium diode (Judson J16-8SP-R05M-HS) after being selected by a 1270 nm band-pass filter (Laser Components, Olching, Germany). Individual traces were accumulated 10-1000 times to improve the signal-to-noise statistics. SODF was monitored at 650 nm, i.e., at the maximum of the porphyrin monomer fluorescence emission band. Because the signals of SODF/$O_2(^1\Delta_g)$ were calculated as differences between the signals at given oxygen concentrations and the detector responses in oxygen-free conditions, the rise part (~0-2 μs) can fail due to the strong prompt fluorescence of the porphyrin photosensitizer and saturation of the detector. The kinetic traces of singlet oxygen phosphorescence were fitted using Equation 1:

$$[O_2(^1\Delta_g)] = A_{SO}\,\tau_\Delta\,[\exp(-t/\tau_T)-\exp(-t/\tau_\Delta)]/(\tau_T-\tau_\Delta), \quad (1)$$

where A is proportional to the quantum yield of $O_2(^1\Delta_g)$, τ_Δ is the lifetime of $O_2(^1\Delta_g)$, and τ_T is the lifetime of the TPP triplets at the given oxygen concentration. Details of the photophysical measurements were described in a previously published paper.[16] All of the photophysical measurements were performed in aqueous media.

(Photo)antibacterial tests

The stock suspension of *E.coli* K-12 (OD_{560} = 0.8) in the LB medium was diluted 10^5 times with PBS (Lonza, Czech Republic). The nanofiber samples (1×1 cm) were placed on bacterial agar plates and inoculated with 20 μL of the diluted suspension of *E. coli*. The agar plates were either illuminated with white light from a 400 W solar daylight simulator (Sol1A Newport, USA) for 15 min or stored in the dark. The nanofiber samples were then immersed in 2 mL of the LB medium and incubated for 4 h at 37°C. Then, 100 μL of this obtained bacterial suspension was inoculated on the agar plates and incubated overnight in darkness at 37°C to allow the individual bacteria to grow and form visible colonies.

Results and Discussion

Preparation and characterization of the anion-exchange nanofiber materials

The pristine electrospun polystyrene material without (**PS**) or with 1 wt % TPP (**PS(TPP)**) in the form of thin membranes (thickness of 0.03 mm) had a basis weight of 2.2-2.3 g m^{-2}, with a mean nanofiber diameter of 270 ± 45 nm.

The anion-exchange material (**AE)** was prepared using a two-step reaction, first sulfonated by chlorosulfonic acid and then treated by ethylenediamine (EDA) to form **AE** with sulfonamide groups (Fig. 1). The reaction sequence attached the functional groups onto the aromatic skeleton and simultaneously cross-linked the polymer, thus ensuring its insolubility in organic solvents.[21]

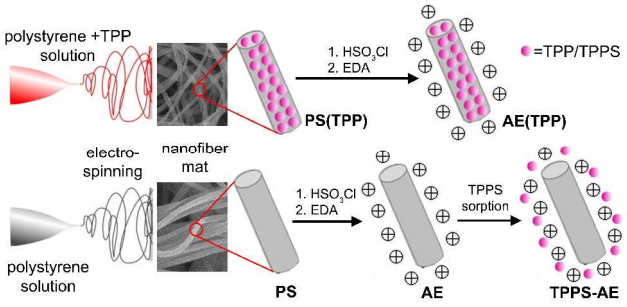

Figure 1. Scheme of preparation of **PS**, **PS(TPP)**, **AE**, **AE(TPP)**, and **TPPS-AE** nanofiber materials.

The nanofiber structure was maintained during these reactions (Fig. 2), and the mean diameter of the **AE** nanofibers increased slightly to 310 nm.

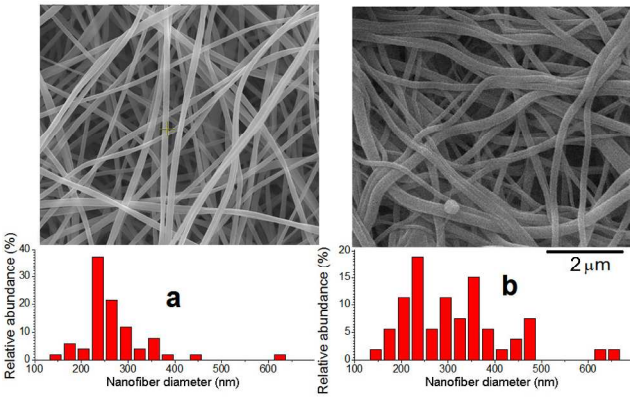

Figure 2. SEM images and nanofiber diameter distribution diagrams of PS (a) and the corresponding AE obtained after 10 min of chlorosulfonation and 10 min of immersion in EDA (b, IEC = 4.0 mmol g^{-1}).

The FTIR spectra of **PS** (Fig. 3a) were consistent with those obtained for the bulk polymer, containing bands at 3000-3100 cm^{-1} (C–H stretching on benzene rings); 2920 cm^{-1} and 2845 cm^{-1} (C–H stretching vibration of the CH_2 and CH groups on the aliphatic polystyrene chain); 1600, 1490, and 1450 cm^{-1} (aromatic C–C stretching); 1024 cm^{-1} (benzene ring in-plane bending); 750 cm^{-1} (benzene ring out-of-plane bending); and 700 cm^{-1} (CH_2 rocking mode).[22] The successful attachment of sulfonamide and sulfone moieties onto the polymeric skeleton resulted in the formation of **AE** with new bands at 1030 and 1090 cm^{-1} (in-plane bending of para-substituted phenyl ring), 1150 cm^{-1} (symmetric SO_2 stretching vibration), and 1310 cm^{-1} (asymmetric SO_2 stretching vibration) and a broad band at 3250 cm^{-1} (N-H stretching) (Fig. 3b).[23, 24]

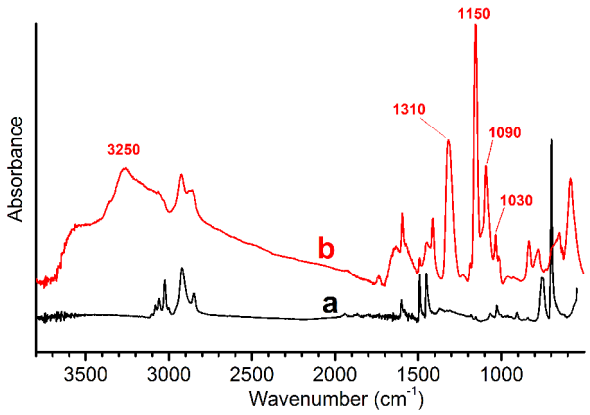

Figure 3. FTIR spectra of PS (a) and AE (b) nanofiber materials; the data are offset.

Ion exchange properties

The ion exchange capacity (IEC) depends on the duration of both reaction steps (Fig. 4, panel A). The maximum IEC values (4.0 mmol g^{-1}) were obtained after 9-13 min immersions in chlorosulfonic acid followed by immersion in EDA. Longer reaction times in both media resulted in the reduction of IEC due to the increased formation of sulfone and amine cross-links[16], whereas shorter immersions did not fully functionalize the polymer.

The anion exchange kinetics of **AE** was tested using TPPS, I_3^- and I^- anions with the same concentration of charges. The adsorption isotherms exhibited a pseudo first-order kinetic behavior (Fig. 4, panel B).[25] The shortest half-time of adsorption was obtained for I_3^- (8.3 min), followed by I^- (33.3 min) and TPPS (46.3 min). Typically, the rate of ion exchange of large organic multivalent anions is slower than that of small univalent inorganic anions.[26]

The bulky I_3^- anion with higher polarizability exhibited higher adsorption affinity than I^-. When **AE** saturated with I^- was immersed in the I_3^- solution, the I_3^- anions replaced I^- on the **AE** surface, as shown by UV-Vis (Fig. S1, ESI†): the absorption bands of I_3^- (287 and 351 nm) in the solution disappeared, whereas the intensity of the I^- absorption band (227 nm) increased. Conversely, the I_3^- was not replaced by I^- even after immersion in 1 M KI.

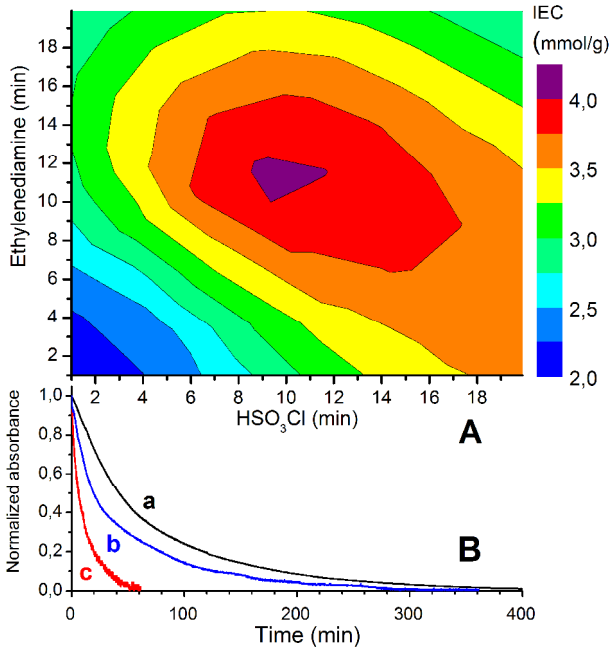

Figure 4. Time dependence of IEC during the functionalization of **PS** by chlorosulfonic acid followed by treatment with EDA (panel A). The kinetics of the adsorption of tetra-anionic 1.6 μM TPPS (a), 6.4 μM I^- (b), and 6.4 μM I_3^- (c) on the **AE** (6 cm^2, 10 mg, IEC = 4.0 mmol/g), aqueous solutions, temperature of 23ºC (panel B).

Preparation of the photoactive anion-exchange materials

We prepared photoactive anion-exchange nanofiber materials with a TPPS photosensitizer adsorbed on the surface of the nanofibers (**TPPS-AE** with TPPS/IES = 0.01). The properties of **TPPS-AE** were compared with the material in which the TPP photosensitizer was encapsulated inside the electrospun nanofibers **PS(TPP)**. The latter material was prepared by electrospinning from polystyrene solution with dissolved TPP and was treated by chlorosulfonic acid (10 min) and EDA (10 min) to form the anion exchange material **AE(TPP)** (Fig. 1). The encapsulated photosensitizer in **PS(TPP)** and **AE(TPP)** was protected from the outer environment by the polymer bulk.

In contrast to the superhydrophobic **PS**[27, 28] and **PS(TPP)** (apparent contact angle ACA = 130 ± 4°), we observed that **AE(TPP)** and **TPPS-AE** (ACA ≤ 5°) were highly hydrophilic (Fig. S2, ESI†) and thus enabled photophysical measurement and photooxidation experiments in aqueous media.

UV-Vis absorption and fluorescence spectra of PS(TPP), AE(TPP), and TPPS-AE

The absorption spectrum of **PS(TPP)** (Fig. 5a, panel A) with a Soret band at 421 nm and four Q bands at 515, 549, 593, and 648 nm was nearly identical to the spectrum of TPP in nonpolar solvents, such as toluene. The absorption bands of **AE(TPP)** were red shifted by 4 nm (Fig. 5b). The red shift in the electronic absorption spectra of TPP can be caused by their

interaction with sulfone or sulfonamide groups[29] rather than by non-planar distortions within the porphyrin molecules.[30]

Extensive aggregation of TPP, which is characterized by broadening of the Soret band or hypochromicity,[31] was not observed for either sample. The absorption spectra of **TPPS-AE** (Fig. 5c) with various TPPS loadings were almost identical to the Soret band at 424 nm and Q bands at 519, 555, 591, and 645 nm. The Soret band of **TPPS-AE** was significantly red shifted (10 nm) compared with that of TPPS in water (Fig. 5d). The spectral shifts of the water-soluble porphyrins in the presence of aromatic compounds have been well documented and are proportional to the energy of association of the aromatics with the porphyrin.[32]

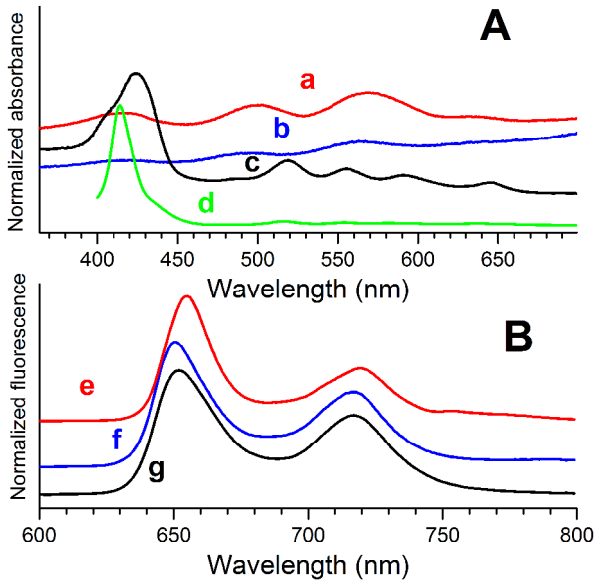

Figure. 5. Panel A: normalized absorption spectra of **PS(TPP)** (a), **AE(TPP)** (b), **TPPS-AE** with TPPS/IES = 0.01 (c) and 10^{-5} M solution of TPPS in water (d); the spectra are offset. Panel B: fluorescence emission spectra of **PS(TPP)** (e), **AE(TPP)** (f), and **TPPS-AE** with TPPS/IES = 0.01 (g), λ_{exc} = 421 nm; the spectra are offset.

The fluorescence emission spectrum of **PS(TPP)** (Fig. 5e, panel B) has band maxima at 655 and 717 nm, which are similar to the bands of TPP dissolved in toluene (656 and 718 nm). The spectrum of **AE(TPP)** (Fig. 5f, panel B) was blue shifted by 4 nm (band maxima at 651 and 713 nm), corresponding to polar changes in the TPP environment. The fluorescence spectrum of **TPPS-AE** was similar to that of **AE(TPP)**, with band maxima at 651 and 717 nm. These observations confirm that photosensitizers encapsulated in polystyrene nanofibers or adsorbed on the surface remain mainly in the monomeric state. The increase of TPPS loading in **TPPS-AE** did not induce any changes in the emission spectra, as recently reported for the surface adsorption of cationic porphyrin TMPyP.[16]

Singlet oxygen, $O_2(^1\Delta_g)$, and triplet states of porphyrins

An important parameter for the efficient photogeneration of $O_2(^1\Delta_g)$ is the diffusion of the oxygen in the ground state to the triplet states of porphyrin. If the quenching of porphyrin triplets by oxygen occurs at or near the diffusion-controlled limit in the polymer, the corresponding Stern-Volmer equation can be expressed by Eq. 2:[12]

$$1/\tau_T = 1/\tau_{T0} + \alpha\,(4\pi N_A \sigma /1000)\, D(O_2)\,[O_2], \qquad (2)$$

where τ_T and τ_{T0} are the triplet lifetimes in air saturated H_2O and oxygen-free media, respectively, α is the probability of quenching in the encounter complex, N_A is Avogadro´s number, σ is the collision diameter of the porphyrin-O_2 complex, $D(O_2)$ is the diffusion coefficient for oxygen, and $[O_2]$ is oxygen concentration.

PS is known for its high diffusion coefficient for oxygen. The quenching of triplet states of encapsulated TPP by oxygen in **PS(TPP)** is highly efficient (Fig. 6a, panel A). The exponential fits to the experimental data reveal lifetimes of TPP triplets ($\tau_0 \sim 2010$ μs in oxygen-free H_2O and $\tau_T \sim 23$ μs in air-saturated H_2O) that correspond to the data of a previous study.[12]

In contrast, the TPP triplets in **AE(TPP)** were largely unaffected by oxygen quenching (Fig. 6a, panel B) with $\tau_0 \sim$ 680 μs and double-exponential kinetics in air-saturated H_2O with $\tau_{T1} \sim 26$ and $\tau_{T2} \sim 605$ μs. The introduction of sulfone and sulfonamide cross-links formed during the post-electrospinning processes into the structure of **AE(TPP)** nanofibers prevents oxygen diffusion towards porphyrin triplet states (eq. 2). Only some of the triplets, located near the nanofiber material surface, were quenched and exhibited identical lifetimes as the TPPS triplets freely accessible to oxygen in **TPPS-AE** (Fig. 6a, panel C, $\tau_0 \sim 440$ μs and $\tau_T \sim 26$ μs).

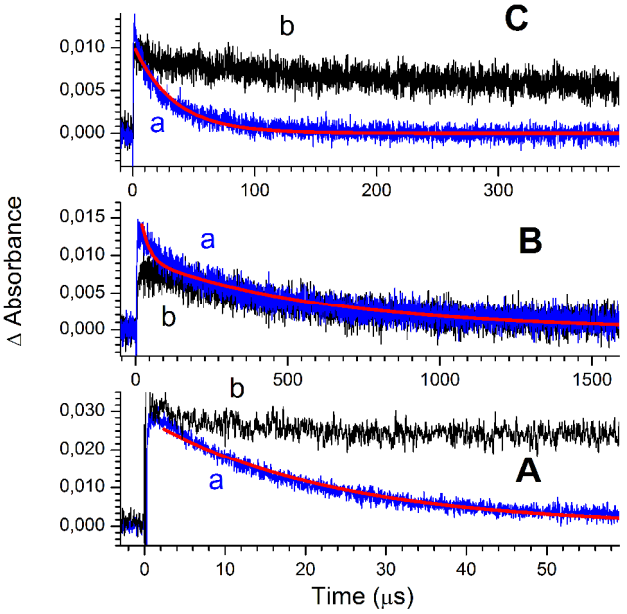

Figure 6. Time-resolved transient absorption of the porphyrin triplet states of **PS(TPP)** (panel A), **AE(TPP)** (panel B), and **TPPS-AE** (panel C, TPPS/IES = 0.01) in the air-saturated H_2O (a) and in the absence of oxygen (b). The traces were recorded at 480 nm following 308 nm pulsed laser excitation by laser flash photolysis in both the transmission and reflection modes. The solid lines represent the exponential fits to the experimental data for the samples in the air-saturated H_2O.

The effect of polystyrene cross-linking on the oxygen permeability has not yet been investigated in detail. Some recent studies of oxygen permeability in polymers have obtained ambiguous conclusions; one study found that the presence of cross-links in glassy PMMA moderately decreased the oxygen permeability,[33] whereas another study found that the oxygen permeability increased with increased cross-linking in ethanol swollen cross-linked PVA.[34]

The formation and kinetics of $O_2(^1\Delta_g)$ were monitored by time-resolved phosphorescence at 1270 nm (Fig. 7, panel A) and singlet oxygen sensitized delayed fluorescence (SODF) at 650 nm (Fig. 7, panel B). SODF is an alternative and sensitive method to monitor both $O_2(^1\Delta_g)$ and triplet porphyrin and occurs via the repopulation of the excited singlet states of the porphyrin photosensitizer due to the reaction of porphyrin triplets with $O_2(^1\Delta_g)$.[19]

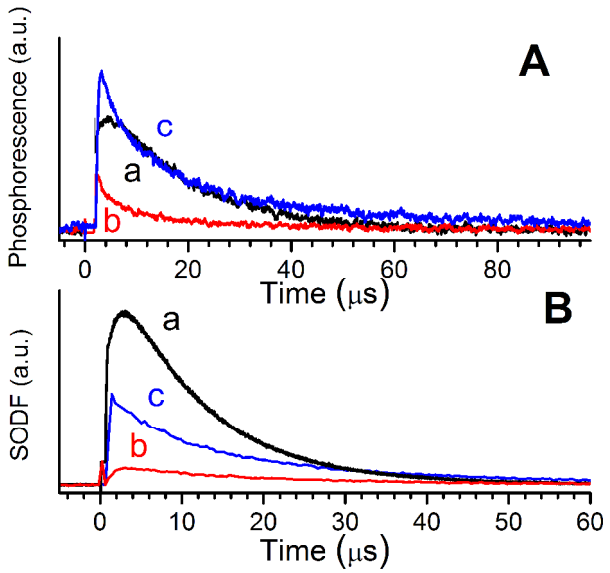

Figure 7. Time-resolved phosphorescence of $O_2(^1\Delta_g)$ at 1270 nm (panel A) and SODF at 650 nm (panel B) of **PS(TPP)** (a), **AE(TPP)PS** (b), and **TPPS-AE** (c, TPPS/IES = 0.01) immersed in air-saturated H_2O (after 308 nm pulsed laser excitation).

The time-resolved phosphorescence intensity plots of nanofiber materials in air-saturated H_2O demonstrate the generation of $O_2(^1\Delta_g)$ of all samples, both anion exchanged materials **TPPS-AE** and **AE(TPP)** and the already reported **PS(TPP)**.[12] It is not easy to compare the efficiency of photogeneration of $O_2(^1\Delta_g)$ due to the lack of homogeneity and different amounts of encapsulated/bounded photosensitizer. Nevertheless, the strong signals of $O_2(^1\Delta_g)$ for **TPPS-AE** (Fig. 7c, panel A) and **PS(TPP)** (Fig. 7a, panel A) correspond to efficient quenching of the triplet states (Fig. 6a, panels C and A), whereas the low signals of **AE(TPP)** (Fig. 7b, panel A) correspond to its low accessibility to oxygen (Fig. 6a, panel B). Accordingly, SODF was the more dominant process for **TPPS-AE** and **PS(TPP)** compared with **AE(TPP)** (Fig. 7 panel B). The intensive SODF of **PS(TPP)** can be attributed to the small distance between the bounded porphyrin molecules and the longer-living $O_2(^1\Delta_g)$ (13.5 μs)[12] in bulk polystyrene, which is the prerequisite for efficient SODF.[19]

The kinetics of $O_2(^1\Delta_g)$ are evidently controlled by the kinetics of the porphyrin triplets. We are unable to precisely calculate the lifetime of $O_2(^1\Delta_g)$ (τ_Δ) from the data presented in Figs. 6 and 7 due to the short τ_Δ in H_2O (~3.5 μs).[35] Alternatively, we performed measurements of $O_2(^1\Delta_g)$ phosphorescence with **TPPS-AE** immersed in D_2O, where τ_Δ is more than one order of magnitude higher.[35] The latter experiment shows $O_2(^1\Delta_g)$ phosphorescence in the solvent (τ_Δ ~ 68 μs) and confirms that $O_2(^1\Delta_g)$ was released into the aqueous phase (Fig. S3, ESI†).

The SODFs of **TPPS-AE** and **AE(TPP)** are highly sensitive to polar external media, in contrast to that of **PS(TPP)** (Fig. 8). The presence of D_2O intensified the SODF signal of **TPPS-AE** because the lifetime of $O_2(^1\Delta_g)$ was increased. In contrast, the presence of NaN_3, an effective quencher of $O_2(^1\Delta_g)$ and porphyrin triplet states,[35] completely quenched the SODF (Fig. 8c, panel A), thus verifying the good accessibility of TPPS triplets to external molecules. Complete SODF quenching was also observed for **AE(TPP)** (Fig. 8b, panel B), where the majority of TPP molecules were located inside of the PS nanofibers and not accessible to the quencher. The quenching of SODF occurred only for the triplets located near the surface. The TPP triplets, buried inside the nanofibers, were unreachable for not only the quencher but also oxygen due to the poor oxygen permeability of the cross-linked **PS**; therefore, no SODF was observed.

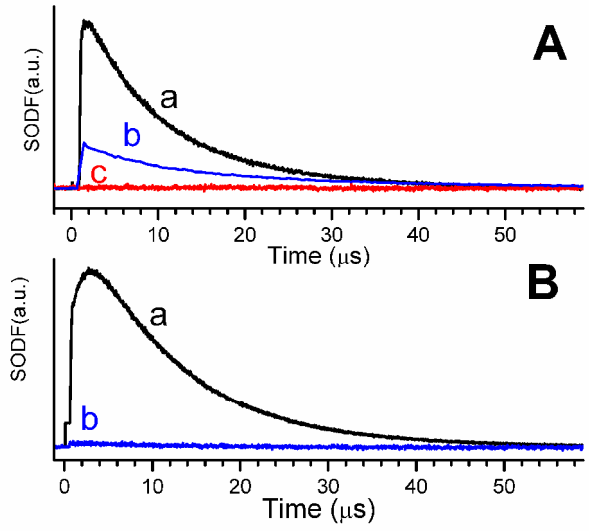

Figure 8. Panel A: Time-resolved SODF kinetics detected at 650 nm of **TPPS-AE** immersed in D_2O (a), water (b), or 0.1 M NaN_3 in H_2O (c). Panel B: Effect of NaN_3 (0.1 M) on the SODF kinetics of **PS(TPP)** (a) and **AE(TPP)** (b).

The mean radial diffusion length of $O_2(^1\Delta_g)$, l_r, can be estimated using the equation $l_r = (6D_0\tau_\Delta)^{1/2}$, where D_0 is the diffusion coefficient for oxygen in water (2.07×10^{-9} m^2s^{-1})[36] and τ_Δ is the lifetime of $O_2(^1\Delta_g)$. The low value of l_r ~ 200 nm for $O_2(^1\Delta_g)$ in H_2O produced by **AE(TPP)** or **TPPS-AE** indicates that the adsorption on the surface or the close contact

of target molecules with nanofibers is a fundamental prerequisite for the effective course of photooxidation reactions. Hence, the electrostatic forces between the nanofibers and substrate can play an important role in the photooxidation and photodynamic processes.

Photooxidation of the external substrates

The ability of $O_2(^1\Delta_g)$ to diffuse outside nanofibers of **TPPS-AE** and **AE(TPP)** was tested by the sensitive method based on the photooxidation of I^-.[37] The photoproduced concentration of I_3^- is proportional to the concentration of $O_2(^1\Delta_g)$. **TPPS-AE** adsorbs I^- on the surface and enables the photooxidation of I^- to I_3^- (Fig. 9, panel A). Some of the I_3^-molecules are also released to the surrounding media, and the concentration increases over time (Fig. 9, panel B). Similar results were observed for the less efficient **AE(TPP)** with a longer irradiation time. The photooxidation efficacy was nearly zero in the presence of 0.1 M NaN_3, which is an effective quencher of $O_2(^1\Delta_g)$. No photooxidation was observed in the dark, upon irradiation in the absence of dissolved oxygen, or upon irradiation of the photosensitizer-free nanofiber materials.

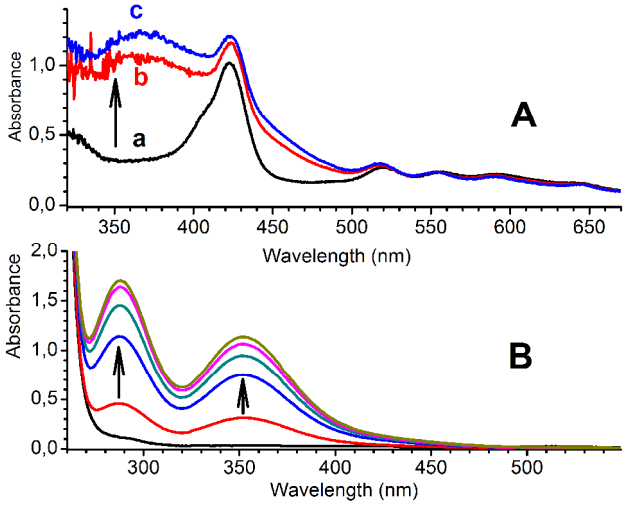

Figure 9. Diffuse-reflectance spectra of **TPPS-AE** (2 cm^2, TPPS/IES = 0.01) containing adsorbed I^- (0.1 µmol) after a) 0, b) 10, and c) 20 min of irradiation; the arrow indicates the spectral changes at ~360 nm, which correspond to I_3^- in less polar media (panel A). The absorption changes of air-saturated aqueous solution of 0.05 M I^- containing a 2 cm^2 piece of **TPPS-AE** during irradiation for 0-15 min; the increasing bands at 287 and 351 nm correspond to photoproduced I_3^- in aqueous media (panel B). The irradiation was performed using a stabilized 300 W halogen lamp at 22°C.

(Photo)antibacterial activity

The surface photo-antibacterial and post-irradiation antibacterial activity of **TPPS-AE** with efficient generation of $O_2(^1\Delta_g)$ was studied using the procedure described in 2.13. Fig. 10 shows the bacterial colonies on agar plates after inoculation with Gram-negative *E.coli* (K-12) from the surface of porphyrin-free **AE** and **TPPS-AE** after 15 min of irradiation (panel B) or in the dark (panel A) and after incubation overnight. Agar plates using inoculum from **TPPS-AE** maintained in the dark and irradiated **AE** were used as the negative controls.

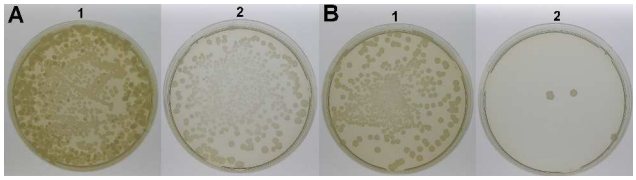

Figure 10. E. coli colonies on agar plates after inoculation from the surface of materials **AE** and **TPPS-AE** kept in the dark (panel A) or irradiated for 15 min (panel B) followed by incubation overnight. Sample 1: **AE**; sample 2: **TPPS-AE** (TPPS/IES = 0.01). Irradiation was performed using a 400 W solar simulator equipped with a water filter.

Bacterial growth was strongly inhibited on the surface of **TPPS-AE** irradiated by simulated daylight, in contrast to both controls (Figs. 10 and 11). Bacterial colonies exhibited limited growth on the agar plates treated with an irradiated sample of **TPPS-AE**. Typically, the average number of CFU decreased from approximately 700 (dark control) to 5 CFU (after the irradiation). This significant antibacterial effect can be attributed to the efficient photogeneration of $O_2(^1\Delta_g)$ on the hydrophilic surface of the nanofibers (ACA $\leq$ 5°) and the electrostatic attraction between the positively charged surface of the nanofibers and bacteria. Bacterial cell surfaces possess a net negative electrostatic charge due to ionized phosphoryl and carboxylate substituents on the outer cell envelope macromolecules, which are exposed to the extracellular environment.[38]

An even stronger photo-antibacterial effect was observed on the surface of **TPPS-AE** (TPPS/IES = 0.01), where the remaining free charges were saturated by I^- (**I-TPPS-AE** material) (Fig. 11). These results are in contrast to porphyrin-free **AE** saturated by I^- (**I-AE**), where a minimal antibacterial effect was observed. These effects can be attributed to the antibacterial I_3^- formed on the surface of the nanofibers based on the photooxidation of I^- by $O_2(^1\Delta_g)$. The antibacterial I_3^- attached on a cationic polymer, such as polyvinylpyrrolidone (povidone), is widely used in medicine as a common antiseptic with broad spectrum antibacterial action for topical application in the treatment and prevention of infection in wounds (e.g., Betadine™, Polydine™, and Jodisol™).

The *in situ* photogenerated I_3^-, an effective antibacterial agent,[39] would prolong the antibacterial effect of the nanofiber materials with porphyrin to the post-irradiation time. **I-TPPS-AE** was irradiated for 15 min to form I_3^- adsorbed on the surface of the nanofibers. The sample was subsequently inoculated with bacterial suspension and kept in contact with the I_3^- enriched **I-TPPS-AE** for the next hour in the dark at 37°C. As a result, the number of CFU decreased to 30% of the initial value in contrast to the control sample (Fig. 11 and Fig. S4, ESI†). No presence of TPPS and/or I_3^- in agar medium was found.

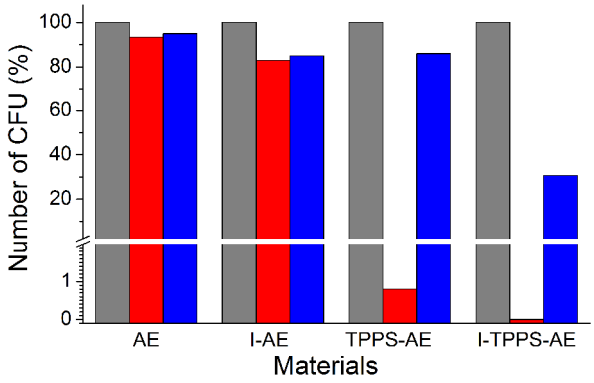

Figure 11. Summary of antibacterial properties expressed as the average number of CFUs as a percentage of the dark control grown after treatment with individual nanofiber samples: stored in the dark (grey columns), irradiated for 15 min (red columns), and stored for 1 h in the dark with pretreated materials (15 min of irradiation, blue columns). Irradiation was performed using a 400 W solar simulator equipped with a water filter.

Conclusions

Herein, we reported the preparation and properties of new photoactive anion exchange polystyrene nanofiber materials with externally bound tetra-anionic TPPS photosensitizers and materials with TPP encapsulated in nanofibers. Both nanofiber materials were highly hydrophilic and exhibited high ion-exchange capacities that could be applied to remove anionic pollutants from the environment. The material with encapsulated TPP exhibited only moderated photogeneration of $O_2(^1\Delta_g)$ due to the limited oxygen permeability of the cross-linked polystyrene matrix. In contrast, the material with externally bounded TPPS exhibited efficient photogeneration of $O_2(^1\Delta_g)$, SODF, oxidation of external substrates, and efficient antibacterial activity when activated by simulated daylight based on the cytotoxic effect of $O_2(^1\Delta_g)$.

To increase the light-induced antibacterial activity and add prolonged dark antibacterial properties, both TPPS and I^- were adsorbed on the surface of the anion exchange polystyrene nanofiber material. Two antibacterial species, $O_2(^1\Delta_g)$ and I_3^-, were simultaneously photogenerated on the surface of the nanofiber materials and can destroy bacteria. Although $O_2(^1\Delta_g)$ has a short lifetime (3.5 μs in H_2O), the long-living I_3^- formed by the photooxidation of I^- with $O_2(^1\Delta_g)$ is responsible for prolonged antibacterial properties in the dark.

Acknowledgements

This work was supported by the Czech Science Foundation (grant number 13-12496S).

References

[a] Faculty of Sciences, Charles University in Prague, Hlavova 2030, 128 43 Prague 2, Czech Republic, phone: +420 221 951 255, e-mail: mosinger@natur.cuni.cz
[b] Center of Applied Bioimplantology, Královské Vinohrady University Hospital, Šrobárova 1150/50, 100 34, Prague 10, Czech Republic.
[c] J. Heyrovský Institute of Physical Chemistry, v.v.i., Academy of Sciences of the Czech Republic, Dolejškova 3, 182 23 Prague 8, Czech Republic.
[d] Institute of Inorganic Chemistry, v.v.i., Academy of Sciences of the Czech Republic, 250 68 Řež, Czech Republic.

† Electronic Supplementary Information (ESI) available: Contact angle measurements and photochemical and antibacterial experiments. See DOI: 10.1039/b000000x/

1 Z. Ma, M. Kotaki and S. Ramakrishna, *J. Membrane Sci.*, 2006, **272**, 179-187.
2 T. Tamura and H. Kawakami, *Nano Letters*, 2010, **10**, 1324-1328.
3 X. Wang, C. Drew, S. Lee, K. J. Senecal, J. Kumar and L. A. Samuelson, *Nano Letters*, 2002, **2**, 1273-1275.
4 H. S. Lim, S. H. Park, S. H. Koo, Y.-J. Kwark, E. L. Thomas, Y. Jeong and J. H. Cho, *Langmuir*, 2010, **26**, 19159-19162.
5 A. Martins, S. Chung, A. J. Pedro, R. A. Sousa, A. P. Marques, R. L. Reis and N. M. Neves, *J. Tissue Eng. Regen. Med.*, 2009, **3**, 37-42.
6 H. S. Yoo, T. G. Kim and T. G. Park, *Adv. Drug Delivery Rev.*, 2009, **61**, 1033-1042.
7 L. T. H. Nguyen, S. Chen, N. K. Elumalai, M. P. Prabhakaran, Y. Zong, C. Vijila, S. I. Allakhverdiev and S. Ramakrishna, *Macromol. Mater. Eng.*, 2013, **298**, 822-867.
8 P. Luana, D. Canan, S. Yewang, Z. Yihui, G. Salvatore, P. Dario, H. Yonggang and A. R. John, *Nat. Commun.*, 2013, **4**, 1633-1633.
9 D. H. Reneker and I. Chun, *Nanotechnology*, 1996, **7**, 216-223.
10 J. Mosinger, O. Jirsák, P. Kubát, K. Lang and B. Mosinger, *J. Mater. Chem.*, 2007, **17**, 164-166.
11 J. Mosinger, K. Lang, P. Kubát, J. Sykora, M. Hof, L. Plíštil and B. Mosinger, *J. Fluoresc.*, 2009, **19**, 705-713.
12 S. Jesenská, L. Plíštil, P. Kubát, K. Lang, L. Brožová, S. Popelka, L. Szatmáry and J. Mosinger, *J. Biomed. Mater. Res. A*, 2011, **99 A**, 676-683.
13 M. Arenbergerova, P. Arenberger, M. Bednar, P. Kubat and J. Mosinger, *Exp. Dermatol.*, 2012, **21**, 619-624.
14 Y. Lhotáková, L. Plíštil, A. Morávková, P. Kubát, K. Lang, J. Forstová and J. Mosinger, *PLoS ONE*, 2012, **7**, e49226.
15 A. Greiner and J. H. Wendorff, *Angew. Chem., Int. Ed.*, 2007, **46**, 5670-5703.
16 P. Henke, K. Lang, P. Kubát, J. Sýkora, M. Šlouf and J. Mosinger, *ACS Appl. Mater. Interfaces*, 2013, **5**, 3776-3783.
17 C. M. Pitsillides, E. K. Joe, X. Wei, R. R. Anderson and C. P. Lin, *Biophys. J.*, 2003, **84**, 4023-4032.
18 M. Gracanin, C. L. Hawkins, D. I. Pattison and M. J. Davies, *Free Radical Biol. Med.*, 2009, **47**, 92-102.
19 J. Mosinger, K. Lang, L. Plíštil, S. Jesenská, J. Hostomský, Z. Zelinger and P. Kubát, *Langmuir*, 2010, **26**, 10050-10056. .
20 K. M. Forward and G. C. Rutledge, *Chem. Eng. J.*, 2012, **183**, 492-503.
21 Cremlyn, R. J. Chlorosulfonic acid: A versatile reagent, 1st ed.; Royal Society of Chemistry: Cambridge, 2002; Chapter 8, pp 250.
22 E. Jabbari and N. A. Peppas, *Macromolecules*, 1993, **26**, 2175-2186.
23 P. K. Gutch, R. K. Srivastava and K. Sekhar, *J. Appl. Polymer Sci.*, 2008, **107**, 4109-4115.
24 R. A. Weiss, A. Sen, C. L. Willis and L. A. Pottick, *Polymer*, 1991, **32**, 1867-1874.
25 S. Azizian, *J. Coll. Interface Sci.*, 2004, **276**, 47-52.

26 K. Matsusaki, N. Hashimoto, N. Kuroki and T. Sata, *Anal. Sci.*, 1997, **13**, 345-349.
27 X. Lu, J. Zhou, Y. Zhao, Y. Qiu and J. Li, *Chem. Mater.*, 2008, **20**, 3420-3424.
28 M. W. Lee, S. An, S. S. Latthe, C. Lee, S. Hong and S. S. Yoon, *ACS Appl. Mater. Interfaces*, 2013, **5**, 10597-10604.
29 J. Bhaumik, R. Weissleder and J. R. McCarthy, *J. Org. Chem.*, 2009, **74**, 5894-5901.
30 A. B. J. Parusel, T. Wondimagegn and A. Ghosh, *J. Am. Chem. Soc.*, 2000, **122**, 6371-6374.
31 K. Procházková, Z. Zelinger, K. Lang and P. Kubát, *J. Phys. Org. Chem.*, 2004, **17**, 890-897.
32 H.-J. Schneider and M. Wang, *J. Org. Chem.*, 1994, **59**, 7464-7472.
33 M. Klinger, L. P. Tolbod, K. V. Gothelf and P. R. Ogilby, *ACS Appl. Mater. Interfaces*, 2009, **1**, 661-667.
34 N. B. Schack, C. L. P. Oliveira, N. W. G. Young, J. S. Pedersen and P. R. Ogilby, *Langmuir*, 2008, **25**, 1148-1153.
35 F. Wilkinson, W. P. Helman and A. B. Ross, *J. Phys. Chem. Reference Data*, 1995, **24**, 663-1021.
36 V. S. Ijeri, K. Daasbjerg, P. R. Ogilby and L. Poulsen, *Langmuir*, 2008, **24**, 1070-1079.
37 J. Mosinger and B. Mosinger, *Experientia*, 1995, **51**, 106-109.
38 W. W. Wilson, M. M. Wade, S. C. Holman and F. R. Champlin, *J. Microbiol. Meth.*, 2001, **43**, 153-164.
39 J. L. Lambert, G. T. Fina and L. R. Fina, *Ind. Eng. Chem. Prod. Res. Dev.*, 1980, **19**, 256-258.